Algorithm assessment for layup defect segmentation from laser line scan sensor based image data

Meister, Sebastian; Wermes, Mahdieu Amin Mahdieu; Stüve, Jan; Groves, Roger M.

DOI
10.1117/12.2558434

Publication date
2020

Document Version
Final published version

Published in
Sensors and Smart Structures Technologies for Civil, Mechanical, and Aerospace Systems 2020

Citation (APA)
Meister, S., Wermes, M. A. M., Stüve, J., & Groves, R. M. (2020). Algorithm assessment for layup defect segmentation from laser line scan sensor based image data. In H. Huang, H. Sohn, & D. Zonta (Eds.), *Sensors and Smart Structures Technologies for Civil, Mechanical, and Aerospace Systems 2020* (Vol. 11379). Article 1137918 (Sensors and smart structures technologies for civil, mechanical, and aerospace systems 2020). SPIE. https://doi.org/10.1117/12.2558434

Algorithm assessment for layup defect segmentation from laser line scan sensor based image data

Meister, Sebastian, Wermes, Mahdieu Amin Mahdieu, Stüve, Jan, Groves, Roger

Sebastian Meister, Mahdieu Amin Mahdieu Wermes, Jan Stüve, Roger M. Groves, "Algorithm assessment for layup defect segmentation from laser line scan sensor based image data," Proc. SPIE 11379, Sensors and Smart Structures Technologies for Civil, Mechanical, and Aerospace Systems 2020, 1137918 (23 April 2020); doi: 10.1117/12.2558434

SPIE.

Event: SPIE Smart Structures + Nondestructive Evaluation, 2020, Online Only, California, United States

Algorithm assessment for layup defect segmentation from laser line scan sensor based image data

Sebastian Meister[a], Mahdieu Amin Mahdi Wermes[a], Jan Stüve[a], and Roger M. Groves[b]

[a] Center for Lightweight Production Technology (ZLP), German Aerospace Center (DLR), Ottenbecker Damm 12, Stade, Germany

[b] Aerospace Non-Destructive Testing Laboratory, Delft University of Technology, Kluyverweg 1, 2629 HS Delft, The Netherlands

ABSTRACT

The Automated Fiber Placement process is established in the aerospace industry for the production of composite components. This technique places several narrow material strips in parallel. Within current industrial Automated Fiber Placement processes the visual inspection takes typically up to 50 % of overall production time. Furthermore, inspection quality highly depends on the inspector. Therefore, automation of visual inspection offers a great improvement potential. To ensure reliable defect detection the segmentation of individual defects must be investigated. For this reason, this paper focusses on an assessment of defect segmentation algorithms. Therefore, 29 structural, statistical and spectral algorithms from related work were assessed, theoretically, using the 12 most relevant criteria as assessed from literature and process requirements. Then, seven most auspicious algorithms were analysed in detail. For reasons of determinism, Neural Network approaches are not part of this paper. Manually labelled prepreg defect images from a laser line scan sensor were used for tests. The test samples contain five defect types with 50 samples of each. Additionally, layups without defects were analysed. It was concluded that *Adaptive Thresholding* works best for global defect segmentation. The *Cell Wise Standard Deviation Thresholding* performs also quite well, but is very sensitive to grid size. Feasible algorithms perform reliable defect segmentation for layed up material.

Keywords: Image Segmentation, Automated Fiber Placement, Inline Inspection, Adaptive Thresholding, Computer Vision, Composite Manufacturing, Laser Line Scan Sensor

1. INTRODUCTION

Lightweight structures are essential in the aerospace industry. Some good examples for an increasing demand on lightweight structural components are the Airbus A350 XWB or Boing 787 wingcover and fuselage manufacturing.[1,2] *Carbon Fiber Reinforced Plastic* (CFRP) offers superior stiffness and strength properties compared to metallic materials. For this reason CFRP is gladly used for lightweight structures. The production of these mostly complex lightweight structures is often quite expensive. To make this process economical, automated, high rate production techniques are necessary. To meet aerospace's high safety requirements a visual inspection step subseqent to the fibre layup is needed.

Nowadays this manually performed inspection takes usually between 32 %[3] to 50 %[4] of overall production time. Furthermore, due to the manual, visual inspection, the inspection quality is sometimes insufficient against the background of the given requirements. This offers great potential for improvements in terms of quality and speed.

One critical aspect during the automated inline inspection is the robust and reliable segmentation of defects within an image. Because a *Laser Line Scan Sensor* (LLSS) is often used in research and development for inline

Further author information: (Send correspondence to Sebastian Meister)
Sebastian Meister: E-mail: sebastian.meister@dlr.de, Telephone: +49 531 295 3710
Mahdieu Amin Mahdi Wermes: E-mail: mahdieu.wermes@dlr.de, Telephone: +49 531 295 3784
Jan Stüve: E-mail: jan.stueve@dlr.de, Telephone: +49 531 295 3700
Roger M. Groves: E-mail: R.M.Groves@tudelft.nl, Telephone: +31 15 27 88230

Sensors and Smart Structures Technologies for Civil, Mechanical, and Aerospace Systems 2020
edited by Haiying Huang, Hoon Sohn, Daniele Zonta, Proc. of SPIE Vol. 11379, 1137918
 · doi: 10.1117/12.2558434

inspection of *Automated Fiber Placement* (AFP) processes, we are focussing on grey scale depth images from a LLSS. A LLSS uses the principle of triangulation to calculate geometrical information from a laser beam which is projected onto a surface and reflected to a camera sensor with a slightly different position than the emitting laser. Because the AFP technique is relatively novel but also getting established in industry, we selected this technique for further investigation of the inspection process.
As Hanbay et al.,[5] Mahajan et al.[6] and Kumar[7] summarised, a lot of research has been done in the field of fabric defect segmentation in the textile industry. Because textiles are somehow very similar to CFRP, research from this field can be very helpful for algorithm selection. Later on Sacco et al.[8] and Zambal et al.[9] published Neural Network based defect detection methods for laser scanner depth images of AFP defects. These methods are working quite well, but face the challenge of determinism and traceability of Neural Network decisions.
Consequentially, missing in this field is a traceable and deterministic algorithm which performs defect segmentation with the sufficient precision, speed and robustness.
Within this postulation we like to focus on rapid defect detection. This is basically the first task in the inspection of composite parts. Prior to the determination of defect types or geometrical measures, as many as possible of the defects have to be found on the manufactured component. For this reason the following research questions are selected for this publication:

Which algorithms are feasible to perform rapid defect detection for previous defined layup defect types?
What is the actual performance of feasible image segmentation methods for this use case?

Regarding these research questions, this paper uses findings from previous fabric defect detection research and investigates these algorithms in the field of AFP defect segmentation. The findings of this publication should be useful for manufacturers of inline inspection systems for AFP processes and will support the certification process of such systems, especially in the aerospace industry.

2. STATE OF THE ART

2.1 Fiber Placement

Various Fiber Placement techniques are currently available on the market. Very common methods are AFP,[10,11] *Dry Fiber Placement* (DFP),[10,11] *Automated Tape Laying* (ATL)[10] and *Direct Roving Placement* (DRP).[12] These processes apply CFRP material layer by layer onto a tool, which is schematically shown in Figure 1[13]
AFP is a technique which is needed to manufacture complex composite structures. Nowadays, this technique gets more and more established in industrial aerospace manufacturing. Because this process is quite novel but also used in industry, we selected this method for further investigations to realise a good transferability of research results. During the AFP process multiple narrow preimpregnated material stripes, so called tows, are placed along a previously programmed path, which is named a course.[14] Each tow is supplied from an individual spool. The supplied material consists of the prepreg material and a release film. The release film is removed during the placement process and stored on another spool. Within the AFP process, composite material e.g. carbon prepreg material is fed into an effector. This effector guides the material to the tools surface. The material is heated at the moment of tow placement to achieve better tack properties.[10] After placing the material, the compaction roller presses the material onto the mold. Each final component consists of many CFRP prepreg layers.[13] Due to parallel heating with a heating system, the material adheres to the tool or previous layer. The AFP process can be used to manufacture various part geometries. Rudberg[15] expects that the AFP method will be used more and more frequently in future applications.
Various defects possibly occur during fibre layup. These defects are often directly related to the lay up process itself.[14] Harik et al.[16] have investigated the link between AFP defects and process planning, layup strategies and machining. Potter[17] has analysed factors for variability in AFP production. Referring to Potter[17] and Harik et al.[16] all defects which can occur during fibre layup result in geometrical changes and deviations from an accurate lay up surface. Common AFP defect types are wrinkles, twists, gaps, overlaps and foreign materials (foil).[14,16,18] These defects are presented schematically in Figure 2. Wrinkles and twists have a different but distinct geometric shape. Gaps and Overlaps are very similar to each other regarding geometrical properties. Due to their similarities, the differentiation between these two defect types is often quite difficult. The thin shape of these defects enables the opportunity to analyse algorithms for this scenario. These defect types are

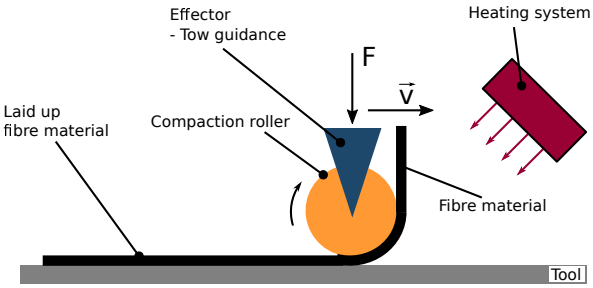

Figure 1: Common basic principle of all fiber placement methods, which consists of an effector with a heating system and compaction roller.

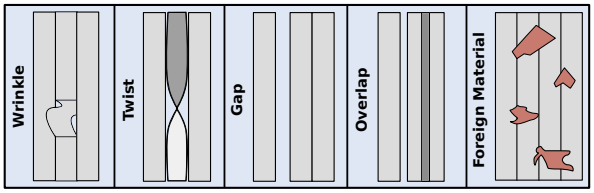

Figure 2: Examples of shape and look of considered defect types.

also often used as exemplary defects by other researchers.[14,16,18,19] Furthermore, foils are very common foreign materials in manufacturing processes.[17,20]

2.2 Sensor technology and Machine Learning

Nowadays, inline inspection for AFP processes is a highly discussed topic in research and industry. InFactory Solutions,[21] Profactor,[22] Electroimpact[23,24] and Danobat Composites[25] have developed LLSS based systems for inline *Quality Assurance* (QA) for AFP processes. Electroimpact uses an individual LLSS system for monitoring each tow. All the other companies mentioned use a single LLSS for inspection of the entire course.
Fraunhofer IIS investigates polarisation camera monitoring systems[26,27] and NASA as well as the *Institute of Production Engineering and Machine Tools - University Hanover* (IFW) focused on thermographic imaging inspection.[28–33] These sensors acquire only 2D image data. The suppliers and industrial developers, mentioned above, have focussed on LLSS based systems. The main advantage of a LLSS system is the ability to measure 3D information, which may be the reason of the success of this measurement technique in this field.[21] In 2007, Schmitt et al.[34,35] started investigations on LLSS based techniques for contour scanning of fabrics and preforms. They also analysed edge detection methods for the detection of misplacement defects of preforms. Schmitt et al. managed to get sub-pixel accuracy for contour measurement and proof that the LLSS is a valid measurement system for fabrics and preforms. Subsequently in 2012 Faidi et al.[36] worked on "Wind Turbine Manufacturing Process Monitoring" in which they investigated laser triangulation systems for CFRP manufacturing. In particular, their aim was the detection and measurement of wires between 0.5 mm and 1 mm which were laminated into CFRP laminates. Miesen et al.[20] suggested a technique to detect defects with a point measurement laser displacement system. In their research they explained influencing factors for deviation and investigates the measurement accuracy of such a system. Furthermore, they showed several defect types and corresponding sizes. Tonnaer et al.[37] also have presented an approach for LLSS based inspection for AFP processes. They analysed the accuracy of edge detection with Otsu's algorithm[38] for defect measurement using LLSS scan data.
Between 2008 and 2016 Hanbay et al.,[5] Mahajan et al.[6] and Kumar[7] have presented plenty of algorithms for fabric defect segmentation mostly without the use of Neural Networks. They all grouped the algorithms basically in structural, statistical and spectral methods as well as other more advanced techniques and have compared their individual strengths and weaknesses. Hanbay et al. have mentioned that especially statistical and spectral analysis methods lead to good fabric defect detection results. They have also pointed out, that spectral techniques work better for regular texture patterns like fabrics. Mahajan et al. have shared this view but also suggests the 9th order Markov Random Field model as an alternative, good performing model based approach. Kumar pointed out, that Gabor filters worked well as an individual method. Combinations of methods however, can lead to even better results.
Another crucial task in the field of image processing is the smoothing of sensor data and intensity value adjustment. The *Contrast Limited Adaptive Histogram Equalization* (CLAHE) algorithm is one feasible technique for image contrast equalisation. It was developed in the mid 80s and was used first by Pizer et al.[39] in the field of medical imaging. Unlike global equalisation techniques, the CLAHE method considers small image areas called "tiles" and performs histogram equalisation for each of these regions. To avoid over amplification of image noise

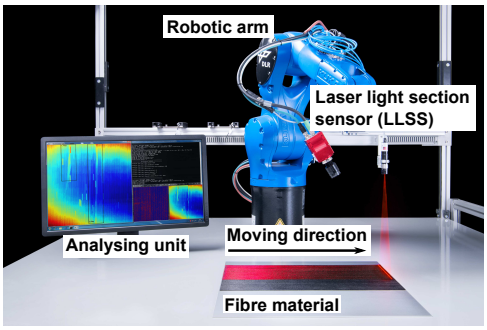

Figure 3: The figure presents the setup for acquisition of defect data from CFRP prepreg material. This setup uses a KUKA Robot with mounted C5 LLSS and performs a linear movement parallel to the lay up surface.

the contrast is limited to a specified value. Pixel values above this relative threshold are shifted to a corresponding neighbour bin.
As mentioned above plenty of algorithms and sensor systems from various fields are already available. Especially algorithms from textile inspection seam feasible to adapt to our use case. Within this publication we like to use a feasible selection of algorithms from textile research and apply them to defect detection on LLSS depth images. Subsequently the methodology to assess these algorithms performances is described.

3. METHODOLOGY

For validation of segmentation algorithms a manageable and heterogeneous set of defect types need to be chosen. Due to the different defect properties mentioned in section 2, we selected wrinkles, twists, gaps, overlaps and foreign materials (foil) as example defects for the experiments. Figure 2 presents these defects. Generally, 'out of data' deviations were not considered in this paper. To assess image analysis methods and classification algorithms, representative data needs to be acquired. This collection of data should be reproducible and representative regarding the actual manufacturing process. For this reason, a setting which is independent from manufacturing influances like heating radiation, undesirable contamination or geometric tilting of the lay up machine is used. A feasible setup is presented in Figure 3. This setup consisted of an articulated robot from KUKA, the *Automation Technology GmbH* (AT) - C5 Sensor[40] and a CFRP prepreg material defect sample which has been mentioned in section 2.1. The AT C5 Sensor acquires 4095 (w) x 500 (h) px, 16-bit grey scale depth images from a 250 x 150 mm fibre layup sample. The image resolution in the width direction is the maximum available sensor resolution. The resolution in the height direction is influenced by the exposure time per pixel row and the time between frames. For this reason the resolution decreases with increasing exposure time. A laser voltage of 5V and the FIR-PEAK laser line detection algorithm[41] was used to acquire the mentioned depth image. The FIR-PEAK algorithm is a derivative filter, which detects the zero crossing point of the first derivative of the laser intensity image. The data capturing is done over ethernet connection using the GenICam protocol.[42] The analysis of these images were performed on a computer with Intel Xeon Gold 5122 @ 3.60 GHz CPU, 48 GB RAM and NVIDIA Quadro P6000 GPU as well as OpenCV 3.4.1[43] with Python. Relevant calculations for analysis were performed on the CPU. The GPU was only used for visualisation. Image capturing was done by a linear robot movement, across the entire length of the defect samples, with a velocity of 200 mm/s.

Various defect segmentation algorithms are available especially from research in fabric defect detection, which have been presented in section 2.2. The mentioned segmentation algorithms were assessed on a theoretical basis with a focus on the overall inline inspection system. This means, that this defect segmentation needs to proceed fast and find most defects, but a less accurate defect segmentation is acceptable. Therefore, nine quantitative performance criteria were specified, weighted and the algorithms were assessed, which is presented in Table 1. This table contains all structural, statistical and spectral algorithms found during the literature review in the computer vision fields medical imaging, autonomous driving and textile inspection. Additionally, the four qualitative criteria 'functional principle', 'algorithms features/ decision criterion', 'estimated sensitivity for defect types' and 'type of invariances' are considered for evaluation. For algorithm selection, we rated algorithms from Table 1 using performance assessments available in literature. The corresponding references are given in the

Table 1: Table for theoretical assessment of defect segmentation algorithms. 29 algorithms from literature were assessed by nine quantitative criteria from related research. The table summarises all algorithms which were found during the literature review. The range of weights goes from unimportant (1) to very important (5). The range of assessment values lies between 0 (no match) and 5 (entirely true). "-" means: Not enough information available. The algorithms which were investigated in this paper are marked in grey.

Criteria

Algorithms	Number of Invariances	Calculation speed	Implementation effort	Detection accuracy	False positive rate	False negative rate	Localising accuracy	Robustness	Adaptability (varying inputs)	**Weighted sum**	Reference
Weights [1-5]	*2*	*5*	*1*	*5*	*3*	*5*	*3*	*4*	*5*		
Edge detection	3	5	4	3	3	4	3	3	3	**3.48**	[44–46]
Region operations	0	4	4	2	2	2	2	2	2	**2.24**	[44–49]
Laplaceian of Gaussian	3	4	4	2	1	1	3	2	2	**2.27**	[44]
Projection (hor./vert.)	1	5	4	4	3	3	4	3	3	**3.45**	[50]
Local Binary Patterns	1	4	4	4	3	4	4	4	2	**3.42**	[51–53]
Principle Comp. Analysis	0	5	4	3	2	2	3	2	1	**2.48**	[52,54]
Linear discr. analysis	0	5	2	3	2	2	3	2	1	**2.42**	[55]
STD per cell thresholding	2	4	4	3	3	4	4	3	2	**3.21**	[5,44]
Histogram approach	2	4	4	3	3	3	1	3	2	**2.78**	[5,44,45]
OTSU	2	5	4	4	3	4	4	3	4	**3.81**	[38,44,56,57]
Adaptive Thresholding	3	5	4	5	5	5	4	4	4	**4.48**	[6,7,44,48,57]
Fractal dimension	1	4	3	4	2	1	1	3	3	**2.61**	[6,7]
First-/ Sec. order statistic	2	4	4	3	3	3	4	3	2	**3.06**	[6]
Texture energy by Laws	0	3	4	3	3	3	2	3	3	**2.76**	[6,58]
Cross correlation analysis	0	3	2	4	2	2	2	3	1	**2.30**	[7]
Auto correlation	0	2	3	4	4	3	1	3	1	**2.42**	[5,53]
Morphological operations	3	4	3	4	4	4	4	3	4	**3.79**	[5,7,44,45,49]
Co-occurrence matrix	1	3	3	4	3	3	3	2	1	**2.61**	[5–7,53]
Eigen filters	0	4	3	3	3	3	1	1	1	**2.24**	[7,59]
Rank-order histogram	2	5	4	3	3	3	3	3	4	**3.42**	[7]
Local linear transforms	0	0	0	0	0	0	0	0	0	**0**	[7]
(Discrete) Fourier Trafo.	3	4	3	4	3	4	1	2	2	**3.00**	[5–7]
Optical Fourier Transform	-	-	-	-	-	-	-	-	-	**-**	[7]
Windowed Fourier Trafo.	3	4	2	4	3	3	3	3	2	**3.12**	[5–7]
Gabor transform	2	4	3	5	4	4	4	4	4	**4.00**	[5–7]
Optimized FIR Filters	1	3	2	4	2	2	4	4	1	**2.67**	[7]
Wigner Distributions	1	1	3	4	2	2	4	3	4	**2.73**	[7]
Wavelet Transform	1	3	2	4	4	4	3	4	2	**3.21**	[5–7]
Hotelling T2 statistic	1	3	1	4	4	4	4	3	2	**3.15**	[60]

right column. Subsequently, we calculated a weighted performance value. The ten algorithms with the greatest performance values, which means a performance value ≥ 3.21, were considered for further investigations. The edge detection with *Gradient Thresholding* (GT), *Image Projection* (IP), *Cell Wise Standard Deviation Thresholding* (CT), *OTSU Thresholding* (OT), AT, *Morphological Segmentation* (MS) and *Gabor Filter Segmentation* (GF) algorithms have been identified for further investigations in this paper. These algorithms are highlighted in Table 1 and were implemented for validation purposes. The basic principle of the algorithms and this selection are briefly explained below.

Due to traceability, it is crucial to use algorithms which can be easily parametrised by simple parameter adjustment and do not require comparative data. For this reason, the Local Binary Patterns segmentation was rejected. The Rank- order histogram technique sorts bins of grey values according to the number of containing pixels. In this way the distribution of pixel values can be displayed but it is not possible to distinguish between areas with and without defects. Furthermore, this is a global criterion that does not allow the localization of prominent areas. For these reasons the Rank- order histogram is not usable for defect detection. The 'cell wise histogram analysis' calculates the statistical measures 'mean' and 'standard deviation' for each individual cell in a large, image-spanning grid. Cells standard deviations greater than a given threshold are marked as conspicuous region, which can be used to estimate and localise defects. With signal evaluation by means of wavelet transformation, some basis function is used to analyse the input signal. For image analysis a matrix with this basis function is shifted over the image and thus individual areas are examined. One popular and easy to use example for a base function is the Gaussian function, which is used for the so called Gabor filtering. For this reason, we selected the OpenCV implementation of the GF,[61] which is also commonly used in fabric inspection.

The GT was implemented by using a Sobel filter. This method performs a convolution operation $G_i = S_i * A$ on the image matrix A in the x and y directions with two individual convolution masks S_i. The results are added up as $G = \sqrt{G_x^2 + G_y^2}$. The edges are estimated applying binary thresholding on matrix G.[62] IP calculates a dimensional reduction vector r_i for each row $r_r(i)$ and each column $r_c(j)$ using $r_i = \sum_{i,j=0}^{n,m}(I(i,j))$.[63] This technique treats each image row/ column as an individual vector and accumulates the corresponding values. Afterwards, a matrix of ones with size equal to the original image $J_{n,m}$ is multiplied by the projection vectors r_i which means $P_r = J_{n,m}r_r$ and $Pc = J_{n,m}r_c$. Subsequently, the overall projection matrix P is calculated by $P = Pr + Pc$ with binary thresholding applied to find the defect areas. OT looks for the threshold t which minimises the variance between two classes, which is defined as the weighted variance of these two classes.[64] Put this as equation $\sigma_w^2(t) = w_0(t)\sigma_0^2(t) + w_1(t)\sigma_1^2(t)$ where w_i are the weights and σ_i are the standard deviations of these classes.[38] AT transforms the input image I(i,j) into a binary image I_b according to $I_b(i,j) = 255$ if $I(i,j) \geq T(i,j)$ otherwise $I_b(i,j) = 0$ with $T(i,j)$ as a pixel wise individual threshold.[64] MS in this paper explains a morphological closing operation which is a dilatation operation followed by an erosion operation like $(I \oplus K) \ominus K$ with input image I and morphological kernel K.[65] To assess the segmentation behaviour, previously acquired data were labeled, manually, with the python tool 'LabelImg'[66] and were used as 'ground truth' for comparison of various algorithms. The validation criteria are similar to the selection criteria from Table 1. For evaluation, 50 defect samples per class were used as the maximum amount of test data currently available. Furthermore, the two best performing algorithms were analysed in detail.

Due to the large number of zero value pixels within the raw image, a pre-processing is necessary, in order to reduce their influences. First the images were dilated to increase the number of information-containing image pixels. With the aim to use the whole available value range a contrast equalisation was performed. To smooth edges from the dilatation step a subsequent Gaussian filtering was performed. Finally the image was resized to a constant size of 1000 x 1000 px. For further analysis the image borders were cropped by 60 px at the top and the bottom as well as 40 px at the left and right edge with aim to compensate for artefacts from the dilatation and filtering steps. In pre-tests the kernel size $k_{size} = 3 \times 3$ was used and the number of dilatation steps were varied between 4 - 12, with aim of finding the best performing configuration. The contrast equalisation was performed with the CLAHE algorithm with variing tile sizes from 5 - 25 px squared. The clipping limit was varied between 2 and 26 to find the best performing configuration. The image padding used the same parameter as the cropping step before, to compensate for the resulting defect position error. These settings has been inspired by configurations from Ma et al.[67] and Muniyappan et al.[68] The Gaussian kernel was set to size $k_{size} = 5 \times 5$ with $\sigma = 0.5$. This raw image pre-processing procedure is presented in the flow chart in Figure 4. Regarding the optimisation approach it is possible, that the pre-processing settings have influences on the decision of the

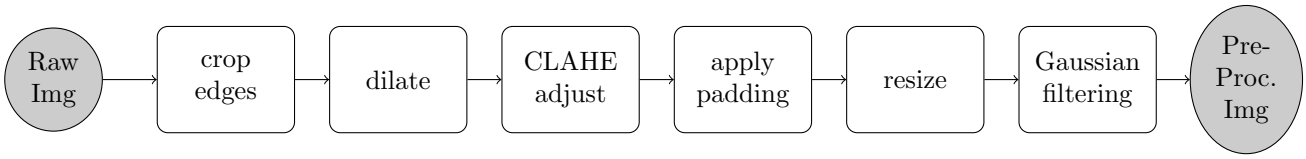

Figure 4: This flow chart shows the sequence of calculations for raw image pre-processing with CLAHE algorithm.

Table 2: The table lists the pre-processing parameter which are modified using specific step size, with aim to find the best parameter configuration for each segmentation algorithm, which generates the best detection results.

Parameter	**Interval**	**Step size**
Dilatation steps	[4,12]	1
CLAHE - Clip Limit	[2,26]	6
CLAHE - Tile size	[5,25]	4
Thresh Img. Dilat. x - Kernel	[3,9]	1
Thresh Img. Dilat. y - Kernel	[3,9]	1
Thresh Img. Dilat. Steps x	[6,12]	2
Thresh Img. Dilat. Steps y	[6,12]	2

actual defect detection algorithms. For this reason, every combination of pre-processing configuration and defect detection algorithm setting was cross checked automatically by the computer. The best performing configuration for the combination of certain pre-processing and segmentation algorithms, considering all defect types, was used for further assessments in this paper. Because the lowest possible number of undetected manufacturing defects is desirable for the manufacturing process, the optimisation criterion was the reduction of undetected defect areas, which means the reduction of false negative values. The investigated defect segmentation step is only the first stage in overall defect analysis within the inspection application. For this reason excess area value up to 100 % can be tolerated. This means, that the segmentation area can be up to twice as large as the labelled 'ground truth' area. This optimisation was performed iteratively for each considered segmentation algorithm. The pre-processing was optimised in parallel to each segmentation algorithm. The optimisation criterion for this step is the maximisation of defect detection accuracy, ideally to the optimum of 100 %. Subsequent to both optimisation steps, the performance of each considered algorithm was determined and compared. The parameters from Table 2 were varied with a given step size to estimate the parameter setting with the best overall detection performance with respect to the previously mentioned optimisation conditions. With the aim to find the best parameter combination, defect detection results were automatically assessed by the computer for every possible parameter combination. The discussed results in this publication are always based on the best performing configuration for each particular case of consideration. The parameters from Table 3 were varied in parallel to the pre-processing configuration with the aim to test every possible parameter combination and to find the best setting for defect segmentation algorithms. For evaluation, eight measurements were analysed, which are related to the literature criteria from Table 1. The calculation time was analysed to reject algorithms with a huge computational time. Defect accuracy and the counter part false negatives rate were investigated to estimate the algorithms detection performance. The false positive values were measured and divided into number based and area based false positive detections to separate between size and counts of these measurements. Regarding correctly detected defects, the excess area and the overlap area were calculated to investigate unnecessary selected data and superfluously marked areas.

4. RESULTS

The individually optimised pre-processing settings from Table 4 and segmentation algorithms from Table 5 were used for all of the following tests. These settings were estimated using the individual optimisation approach described above and specified in Table 3. Figure 5 graphically represents the calculation times for each selected algorithm from Table 6. The MS, AT and OT performed the segmentation swiftest. They need less then 31 ms for *Full Image* (FI) implementation and less then 10 ms for *Grid Based* (GB) implementation per input image. The GF performes most unpalatably with a mean calculation time of greater than 300 ms. Figure 6 shows the

Table 3: The table presents the variations of detect detection algorithms configurations.

Algorithm	**Parameter**	**Interval**	**Step size**
GT	Kernel size sobel filter	[3,7]	2
	Sobel threshold x	[120,150]	10
	Sobel threshold y	[120,150]	10
CT	Cell size x	[10,40]	10
	Cell size y	[10,40]	10
	Cell overlap	[0,0.5]	0.5
	Threshold STD	[4,10]	1
IP	Numb. rot. x	[0,3]	1
	Threshold	[90,140]	10
OT	None	None	None
AT	Thresh. Offset	[-40,-10]	4
GF	Kernel size x	[7,31]	4
	σ	[1,10]	1
	λ	[1,10]	1
	Threshold Gabor filter	[5,10]	1

Table 4: The table shows the calculated best performing image pre-processing parameter configuration for each detection algorithm using a combination of dilatation and CLAHE algorithm.
Legend: Single values: < FI = GB > | Different values < FI >;< GB > | " same value as cell above

Algorithms \ **Parameter**	Dilatation steps	CLAHE - Clip Limit	CLAHE - Tile size	Thresh Img. Dilat. x - Kernel	Thresh Img. Dilat. y - Kernel	Thresh Img. Dilat. Steps x	Thresh Img. Dilat. Steps y
GT	4	20;2	(8,8)	(9,1)	(1,3)	6;10	8
CT	4	26;14	"	"	"	6	"
IP	12;6	26;2	"	"	"	6	"
OT	6;12	2;14	"	"	"	6	"
AT	8;12	20	"	"	"	12;6	"
GF	12	26	"	"	"	12	"
MS	10	14	"	"	"	6	"

Table 5: The table presents the variations of defect detection algorithms configurations which were used for tests. The same configuration was used for FI and GB.

Algorithm	**Parameter**	**Configuration**
GT	Kernel size sobel filter	5
	Sobel threshold x	130
	Sobel threshold y	140
CT	Cell size x	10
	Cell size y	10
	Cell overlap	0.5
	Threshold STD	7
IP	Numb. rot. x	1
	Threshold	130
OT	None	None
AT	Thresh. Offset	-20
GF	Kernel size x	31
	σ	10
	λ	10
	Threshold Gabor filter	10
MS	None	None

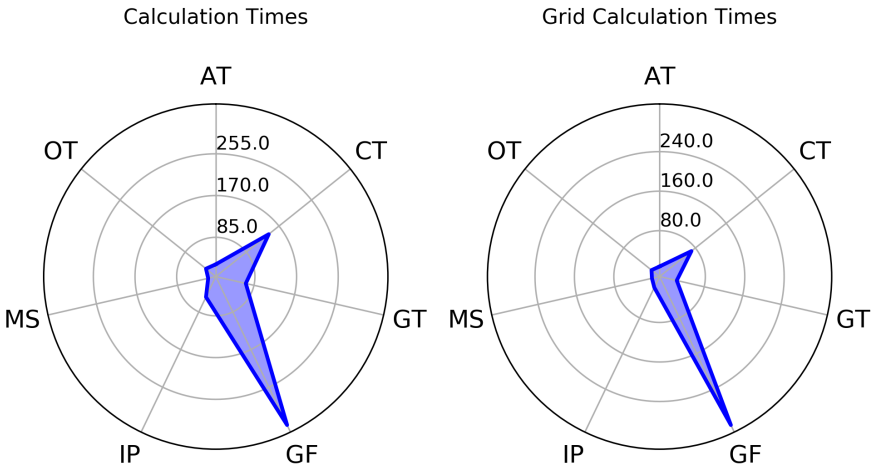

Figure 5: The radar charts compare the calculation times in Milliseconds [ms] of each individual detection algorithm.

Table 6: The table presents the calculation times and standard deviations in Milliseconds [ms] for all considered algorithms for FI and GB configuration.

	Calculation time [ms]	
Algorithm	FI	GB
GT	67.9 ($\sigma = 3.9$)	22.9 ($\sigma = 1.0$)
CT	143.4 ($\sigma = 8.4$)	69.8 ($\sigma = 0.6$)
IP	51.3 ($\sigma = 3.9$)	11.8 ($\sigma = 1.0$)
OT	30.7 ($\sigma = 3.2$)	8.0 ($\sigma = 1.6$)
AT	30.0 ($\sigma = 4.0$)	7.6 ($\sigma = 0.1$)
GF	340.5 ($\sigma = 49.3$)	320.6 ($\sigma = 8.6$)
MS	21.0 ($\sigma = 1.9$)	3.0 ($\sigma = 0.6$)

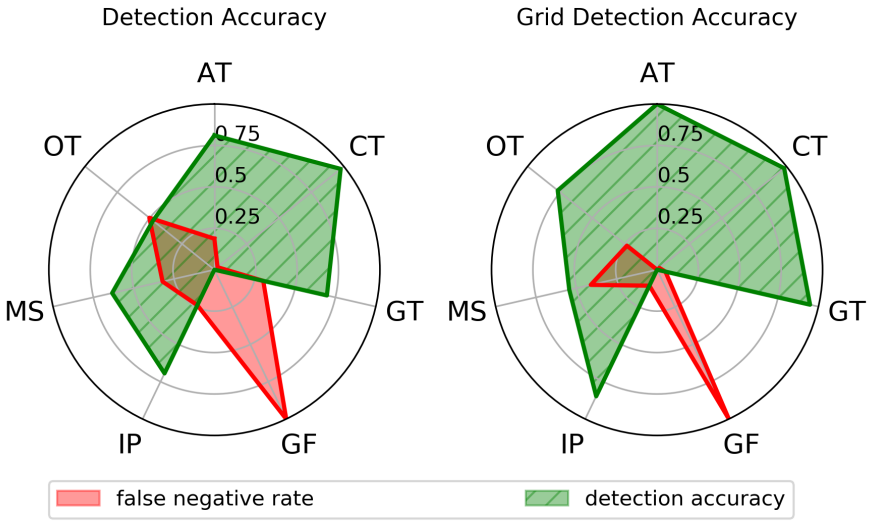

Figure 6: Radar charts for comparison of FI and GB detection accuracies and corresponding false negative rates with individual best performing pre-processing, considering all defect types. Co-Domain: [0,1]

Table 7: Defect detection results for AT and CT are presented in detail, considering all defects. The values are given in %

	FI AT	GB AT	FI CT	GB CT
Detection accuracy	81.0 ($\sigma = 28.5$)	100.0 ($\sigma = 0.0$)	97.6 ($\sigma = 6.1$)	98.2 ($\sigma = 4.1$)
Position accuracy	67.9 ($\sigma = 28.8$)	77.9 ($\sigma = 24.5$)	76.8 ($\sigma = 24.3$)	77.9 ($\sigma = 24.5$)
False neg. rate	18.7 ($\sigma = 28.4$)	0.0 ($\sigma = 0.0$)	2.4 ($\sigma = 6.1$)	1.8 ($\sigma = 4.1$)
False pos. rate (Number)	22.3 ($\sigma = 20.3$)	44.2 ($\sigma = 33.3$)	29.2 ($\sigma = 23.5$)	35.7 ($\sigma = 30.4$)
False pos. rate (area)	3.1 ($\sigma = 0.9$)	8.7 ($\sigma = 4.6$)	14.8 ($\sigma = 6.2$)	11.8 ($\sigma = 4.8$)
Excess area	64.1 ($\sigma = 16.2$)	69.0 ($\sigma = 24.2$)	61.4 ($\sigma = 22.4$)	68.3 ($\sigma = 16.8$)
Overlap area	11.6 ($\sigma = 10.6$)	9.0 ($\sigma = 10.1$)	9.9 ($\sigma = 9.1$)	15.7 ($\sigma = 11.6$)

results for defect accuracies and false negative rates when considering all defect data. We see that the AT and CT algorithms in the FI and the GB implementations perform best for the experimental setup. The 5th most precise algorithm is the FI GT algorithm. All the other algorithms show detection rates below 50 %, which is not usable for this application. For this reason, we focus on the AT and CT algorithms in both variations, for further investigation in this paper.

Subsequently both variants of AT and CT are investigated in detail, due to the good segmentation results in all considered cases. Figure 7 shows the test results for these two segmentation techniques. The results of both techniques are presented in Table 7. The GB AT algorithm shows the best overall detection result with 100 % detection accuracy, followed by GB CT algorithms with 98.2 % ($\sigma = 4.1$ %) detection accuracy. A similar result can be seen for the defect position accuracy. Therefore the GB AT and both CT algorithms show position accuracies around 78 % followed by the FI AT algorithm with a position accuracy around 68 %. Surprisingly, the number based false positives rates are much lower for both FI implementations than for the GB implementations. Furthermore, it is notable, that the average ground truth regions and the automatically segmented areas do only overlap by around 15 % for both methods, but the excess area for detected defects is quite high.

Especially the detection results for the analysis of all considered defects are much better than for the competing algorithms. For an inspection application the region of interest would need to be enlarged artificially.

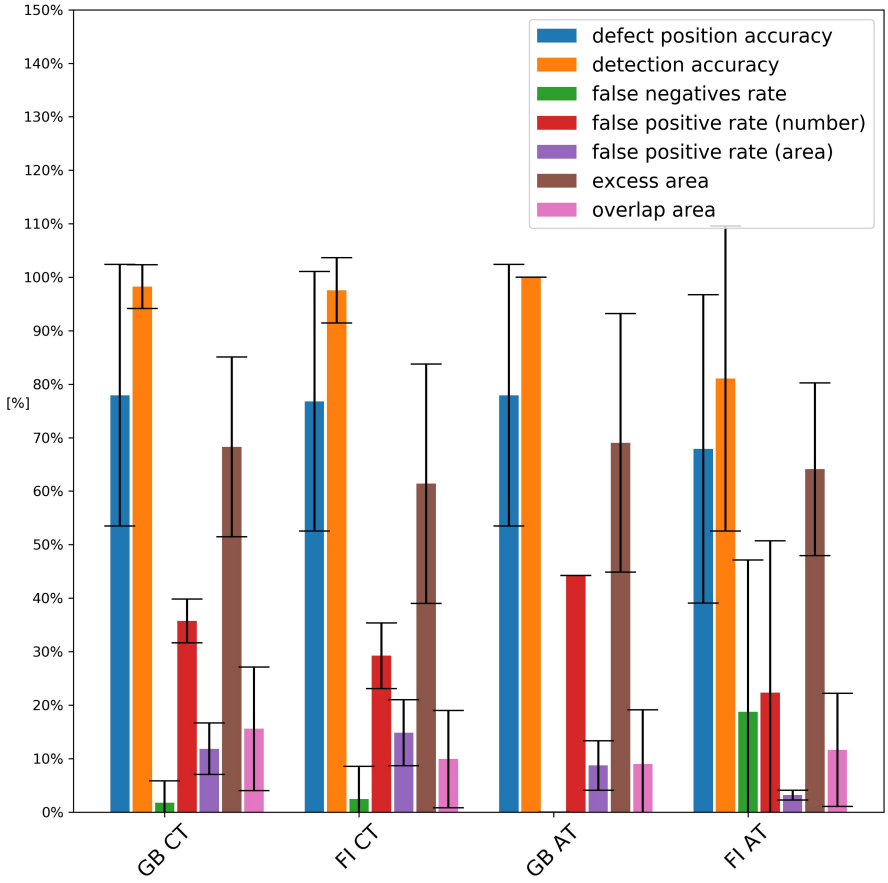

Figure 7: Detection results for best performing algorithms AT and CT considering all defect types. The bars represent the standard deviation.

5. DISCUSSION

In comparison to the Neural Network based defect detection results from e.g. Schmidt et. al,[31,32] the classical image segmentation techniques mentioned in this paper generate very usable results. The selected segmentation algorithms from fabric inspection worked quite well except the GF algorithms, which produce bad detection results. Regarding this issue, Hanbay et al.[5] mentioned in their work that GF is only feasible for relatively uniform structured image data. The prepreg material LLSS data in this publication contains not evenly distributed artefacts. Taking this effect into account, the behaviour of the GF algorithms is comprehensible. The OT algorithms also deliver a weaker performance compared to Tonnaer et al.[37] This is probably caused by the brightness gradient in the image, which causes the algorithms to segment a very large image area. An improved pre-processing which is more tolerant for changes in brightness may reduce this issue. It should also be noted, that the CLAHE image adjustment algorithm is very sensitive to the assigned settings, particularly with regard to its 'clip limit'. The clip limit is a previously defined value. The area of the histogram above this clip limit is distributed over the entire base of the histogram and thus adjusts the resulting image histogram. In general it can be seen that pre-processing is crucial in terms of noise reduction. This step needs to be adjusted individually for each setup and production process.

With regard to the research questions, it should be noted, that the AT and CT algorithms are feasible for defect detection for CFRP prepreg material. The GT algorithms also perform acceptably defect detection results but only for geometrically larger defects or as GB implementation.

For most cases AT and CT show detection accuracies > 95 % and for protruding defects even up to 100 % mean detection accuracy. The positioning accuracy estimates defect position with acceptable accuracy with mostly less

than 30 % deviation from labelled ground truth defect position. Unfortunately, the actual defect segmentation with regard to segmentation area is much worse, for both overlap and excess area.
In future work, the influences of various materials and changing LLSS settings needs to be investigated. Especially varying optical material properties can have an impact on some algorithms. For this reason, these optical material properties will need to be investigated and linked to the previous findings. Furthermore a detailed analysis of the defect detection performance for individual defect types or geometrical groups of defects need to be investigated. In addition it should be mentioned, that the pre-processing can be optimised for better performance, which was not part of this publication, as mentioned above.

6. CONCLUSION

In summary, it can be stated that *Grid Based Adaptive Thresholding* and both *Cell Wise Standard Deviation Thresholding* implementations enable detection accuracies > 97 % with defect position accuracies > 75 %. It is worth noting that the algorithm performance is highly influenced by the pre-processing or rather the input data. For this reason, the pre-processing step needs to be adjusted for each material, process, sensor and algorithm, individually. The segmentation of particular defect regions performs even worse with overlapping below 20 % in average, which is a noteworthy result.

REFERENCES

1. G. Marsh, "Airbus A350 XWB update," *Reinforced Plastics* **54**, pp. 20–24, Nov. 2010.
2. A. McIlhagger, E. Archer, and R. McIlhagger, "Manufacturing processes for composite materials and components for aerospace applications," in *Polymer Composites in the Aerospace Industry*, pp. 59–81, Elsevier, 2020.
3. T. Rudberg, J. Nielson, M. Henscheid, and J. Cemenska, "Improving AFP cell performance," *SAE International Journal of Aerospace* **7**, pp. 317–321, Sept. 2014.
4. C. Eitzinger, "Inline inspection helps accelerate production by up to 50 %," *Lightweight Design worldwide* , Mar. 2019.
5. K. Hanbay, M. F. Talu, and Ömer Faruk Özgüven, "Fabric defect detection systems and methodsa systematic literature review," *Optik* **127**(24), pp. 11960–11973, 2016.
6. P. Mahajan, S. Kolhe, and P. Patil, "A review of automatic fabric defect detection techniques," *Advances in Computational Research* **1**, Jan. 2009.
7. A. Kumar, "Computer-vision-based fabric defect detection: A survey," *IEEE Transactions on Industrial Electronics* **55**, pp. 348–363, Jan. 2008.
8. C. Sacco, A. B. Radwan, R. Harik, and M. V. Tooren, "Automated fiber placement defects: Automated inspection and characterization," in *SAMPE 18 - Long Beach*, p. 13, (McNAIR Center for Aerospace Innovation and Research, Department of Mechanical Engineering, College of Engineering and Computing, University of South Carolina 1000 Catawba St., Columbia, SC, 29201, USA), 2018.
9. S. Zambal, C. Heindl, C. Eitzinger, and J. Scharinger, "End-to-end defect detection in automated fiber placement based on artificially generated data," in *Fourteenth International Conference on Quality Control by Artificial Vision*, C. Cudel, S. Bazeille, and N. Verrier, eds., SPIE, July 2019.
10. H. Lengsfeld, F. W. Fabris, J. Krmer, J. Lacalle, and V. Altstdt, *Faserverbundwerkstoffe*, Hanser Fachbuchverlag, 2014.
11. D. Maass, "Automated dry fiber placement for aerospace composites," in *Composites Manufacturing 2012*, Danobat, Mar. 2012.
12. Y. Grohmann, N. Stoffers, A. Kühn, and T. Mahrholz, "Development of the direct roving placement technology (DRP)," in *ECCM17 - 17th European Conference on Composite Materials*, June 2016.
13. F. Campbell, *Manufacturing Processes for Advanced Composites*, Elsevier Science & Technology, 2004.
14. E. Oromiehie, B. G. Prusty, P. Compston, and G. Rajan, "Automated fibre placement based composite structures: Review on the defects, impacts and inspections techniques," *Composite Structures* **224**, p. 110987, sep 2019.

15. T. Rudberg, "Webinar: Building AFP system to yield extreme availability." CompositesWorld, Apr. 2019. Video.
16. R. Harik, C. Saidy, S. J. Williams, Z. Gurdal, and B. Grimsley, "Automated fiber placement defect identity cards: cause, anticipation, existence, significance, and progression," in *SAMPE 18*, 01 2018.
17. K. Potter, "Understanding the origins of defects and variability in composites manufacture," *ICCM International Conferences on Composite Materials* , 01 2009.
18. F. Heinecke and C. Willberg, "Manufacturing-induced imperfections in composite parts manufactured via automated fiber placement," *Journal of Composites Science* **3**, p. 56, June 2019.
19. Z. Gurdal, B. Tatting, and K. Wu, "Tow-placement technology and fabrication issues for laminated composite structures," in *46th AIAA/ASME/ASCE/AHS/ASC Structures, Structural Dynamics and Materials Conference*, American Institute of Aeronautics and Astronautics, Apr. 2005.
20. N. Miesen, J. Sinke, R. M. Groves, and R. Benedictus, "Simulation and detection of flaws in pre-cured CFRP using laser displacement sensing," *The International Journal of Advanced Manufacturing Technology* **82**, pp. 341–349, June 2015.
21. C. Weimer, A. Friedberger, A. Helwig, S. Heckner, C. Buchmann, and F. Engel, "Increasing the productivity of CFRP production processes by robustness and reliability enhancement," in *CAMX 2016 - The Composites and Advanced Materials Expo and Conference*, (Airbus Group Innovations, 81663 Munich, Germany; AirbusInfactory Solutions GmbH, 81663 Munich, Germany), Sept. 2016.
22. G. Gardiner, "Zero-defect manufacturing of composite parts." CompositesWorld, Nov. 2018. https://www.compositesworld.com/blog/post/zero-defect-manufacturing-of-composite-parts.
23. S. Black, "Improving composites processing with automated inspection." compositesworld, Jan. 2018. https://www.compositesworld.com/articles/improving-composites-processing-with-automated-inspection.
24. J. Cemenska, T. Rudberg, and M. Henscheid, "Automated in-process inspection system for AFP machines," *SAE International Journal of Aerospace* **8**, pp. 303–309, Sept. 2015.
25. S. Black, "Improving composites processing with automated inspection, part II." compositesworld, June 2018. https://www.compositesworld.com/articles/improving-composites-processing-with-automated-inspection.
26. M. Schöberl, K. Kasnakli, and A. Nowak, "Measuring strand orientation in carbon fiber reinforced plastics (CFRP) with polarization," in *19th World Conference on Non-Destructive Testing 2016*, 2016.
27. G. A. Atkinson, T. J. Thornton, D. I. Peynado, and J. D. Ernst, "High-precision polarization measurements and analysis for machine vision applications," in *2018 7th European Workshop on Visual Information Processing (EUVIP)*, IEEE, Nov. 2018.
28. P. D. Juarez, K. E. Cramer, and J. P. Seebo, "Advances in in situ inspection of automated fiber placement systems," in *Thermosense: Thermal Infrared Applications XXXVIII*, J. N. Zalameda and P. Bison, eds., SPIE, May 2016.
29. E. D. Gregory and P. D. Juarez, "In-situ thermography of automated fiber placement parts," in *AIP Conference Proceedings*, Author(s), 2018.
30. C. Schmidt, B. Denkena, T. Hocke, and K. Vltzer, "Influence of afp process parameters on the temperature distribution used for thermal in-process monitoring," *Procedia CIRP* **66**, pp. 68 – 73, 2017. 1st CIRP Conference on Composite Materials Parts Manufacturing (CIRP CCMPM 2017).
31. C. Schmidt, T. Hocke, and B. Denkena, "Artificial intelligence for non-destructive testing of CFRP prepreg materials," *Production Engineering* , July 2019.
32. C. Schmidt, T. Hocke, and B. Denkena, "Deep learning-based classification of production defects in automated-fiber-placement processes," *Production Engineering* **13**, pp. 501–509, Mar. 2019.
33. B. Denkena, C. Schmidt, K. Vltzer, and T. Hocke, "Thermographic online monitoring system for automated fiber placement processes," *Composites Part B: Engineering* **97**, pp. 239–243, July 2016.
34. R. Schmitt, C. Niggemann, and C. Mersmann, "Contour scanning of textile preforms using a light-section sensor for the automated manufacturing of fibre-reinforced plastics," in *Optical Sensors 2008*, F. Berghmans, A. G. Mignani, A. Cutolo, P. P. Meyrueis, and T. P. Pearsall, eds., **7003**, pp. 436 – 447, SPIE, Apr. 2008.

35. R. Schmitt, A. Orth, and C. Niggemann, "A method for edge detection of textile preforms using a light-section sensor for the automated manufacturing of fibre-reinforced plastics," in *Optical Measurement Systems for Industrial Inspection V*, W. Osten, C. Gorecki, and E. L. Novak, eds., SPIE, June 2007.
36. W. Faidi, C. Nafis, S. Sinha, C. Yerramalli, A. Waas, S. Advani, J. Gangloff, and P. Simacek, "Wind turbine manufacturing process monitoring," tech. rep., General Electric Global Research Center, Apr. 2012.
37. R. Tonnaer, S. Shroff, and R. Groves, "Online preventive non-destructive evaluation for automated fibre placement," in *3rd International Symposium on Composite Manufacturing*, pp. 114–123, 2017.
38. N. Otsu, "A threshold selection method from gray-level histograms," *IEEE Transactions on Systems, Man, and Cybernetics* **9**, pp. 62–66, Jan. 1979.
39. S. M. Pizer, J. D. Austin, J. R. Perry., H. D. Safrit, and J. B. Zimmerman, "Adaptive histogram equalization for automatic contrast enhancement of medical images," in *Application of Optical Instrumentation in Medicine XIV and Picture Archiving and Communication Systems*, S. J. D. III and R. H. Schneider, eds., **0626**, pp. 242 – 250, SPIE, June 1986.
40. Automation Technology GmbH, "C5 series - user manual for high speed 3d sensors," techreport 1.2, Automation Technology GmbH, Hermann-Bssow-Strae 6-8, 23843 Bad Oldesloe, Germany, Mar. 2019. Rev 1.2.
41. Automation Technology GmbH, "The FIR filter," techreport 1.0, Automation Technology GmbH, Hermann-Bssow-Strae 6-8, 23843 Bad Oldesloe, Germany, Apr. 2014. Rev. 1.0.
42. European Machine Vision Association, "Emva genicam standard," techreport 2.0, European Machine Vision Association (EMVA), Nov. 2009. Release 2.0.
43. G. Bradski, "The OpenCV Library," *Dr. Dobb's Journal of Software Tools* , 2000.
44. L. K. Lee, S. C. Liew, and W. J. Thong, "A review of image segmentation methodologies in medical image," in *Lecture Notes in Electrical Engineering*, pp. 1069–1080, Springer International Publishing, Nov. 2014.
45. H. Kaur and D. R. Sharma, "A survey on techniques for brain tumor segmentation from MRI," *IOSR Journal of Electronics and Communication Engineering* **11**, pp. 01–05, May 2016.
46. N. Dhanachandra and Y. J. Chanu, "A survey on image segmentation methods using clustering techniques," *European Journal of Engineering Research and Science* **2**, p. 15, Jan. 2017.
47. M. Neubert and G. Meinel, "Evaluation of segmentation programs for high resolution remote sensing applications," 2003.
48. S. Masood, M. Sharif, A. Masood, M. Yasmin, and M. Raza, "A survey on medical image segmentation," *Current Medical Imaging Reviews* **11**, pp. 3–14, Apr. 2015.
49. M. A. H. Ibtihal D. Mustafa, "A comparison between different segmentation techniques used in medical imaging," *American Journal of Biomedical Engineering* **6**(2), pp. 59–69, 2016.
50. A. Kumar and G. Pang, "Defect detection in textured materials using Gabor filters," *IEEE Transactions on Industry Applications* **38**(2), pp. 425–440, 2002.
51. F. Tajeripour, E. Kabir, and A. Sheikhi, "Fabric defect detection using modified local binary patterns," *EURASIP Journal on Advances in Signal Processing* **2008**, Nov. 2007.
52. Z. Liu, L. Yan, C. Li, Y. Dong, and G. Gao, "Fabric defect detection based on sparse representation of main local binary pattern," *International Journal of Clothing Science and Technology* **29**(3), pp. 282–293, 2017.
53. X. Xie, "A review of recent advances in surface defect detection using texture analysis techniques," *ELCVIA Electronic Letters on Computer Vision and Image Analysis* **7**, p. 1, June 2008.
54. P. M. Shanbhag and M.P.Deshmukh, "Fabric defect detection using principal component analysis," in *International Journal of Engineering Research & Technology*, **2**, IJERT, Sept. 2013.
55. ALGLIB-Project, "Linear discriminant analysis." ALGLIB - numerical analysis library. Accessed: 2019-06-1.
56. H.-F. Ng, "Automatic thresholding for defect detection," in *Third International Conference on Image and Graphics (ICIG04)*, IEEE, 2004.
57. A. Norouzi, M. S. M. Rahim, A. Altameem, T. Saba, A. E. Rad, A. Rehman, and M. Uddin, "Medical image segmentation methods, algorithms, and applications," *IETE Technical Review* **31**, pp. 199–213, May 2014.
58. S. Meister, S. Kaestner, and C. Krombholz, "Enhancements of an inline QA system for fiber layup processes," in *ISCM 2018*, Nov. 2018.

59. P. Cattin, "Texture segmentation - introduction to signal and image processing." MIAC, University of Basel, May 2016. Accessed: 2019-06-17.
60. H.-D. Lin, "Computer-aided visual inspection of surface defects in ceramic capacitor chips," *Journal of Materials Processing Technology* **189**, pp. 19–25, July 2007.
61. OpenCV, "Image processing - Image Filtering," techreport, OpenCV, Feb. 2018.
62. OpenCV, "Image Processing (imgproc module) - Sobel Derivatives," techreport, OpenCV, Aug. 2019.
63. OpenCV, "OpenCV API Reference - Operations on Arrays - Reduce," techreport, OpenCV, Dec. 2019.
64. OpenCV, "Image Thresholding," techreport, OpenCV, Feb. 2018.
65. OpenCV, "Morphological Transformations," techreport, OpenCV, Feb. 2018.
66. Tzutalin, "LabelImg." https://github.com/tzutalin/labelImg, 2015. https://github.com/tzutalin/labelImg.
67. J. Ma, X. Fan, S. X. Yang, X. Zhang, and X. Zhu, "Contrast Limited Adaptive Histogram Equalization Based Fusion for Underwater Image Enhancement," Mar. 2017.
68. S. Muniyappan, A. Allirani, and S. Saraswathi, "A novel approach for image enhancement by using contrast limited adaptive histogram equalization method," in *2013 Fourth International Conference on Computing, Communications and Networking Technologies (ICCCNT)*, IEEE, July 2013.